



HAL
open science

Design of lanthanide-based metal–organic frameworks with enhanced near-infrared emission

Tu Nguyen, Svetlana Eliseeva, Andrzej Gladysiak, Stephane Petoud, Kyriakos Stylianou

► **To cite this version:**

Tu Nguyen, Svetlana Eliseeva, Andrzej Gladysiak, Stephane Petoud, Kyriakos Stylianou. Design of lanthanide-based metal–organic frameworks with enhanced near-infrared emission. *Journal of Materials Chemistry A*, 2020, 8 (20), pp.10188-10192. 10.1039/d0ta01677b . hal-02935790

HAL Id: hal-02935790

<https://hal.science/hal-02935790>

Submitted on 16 Nov 2020

HAL is a multi-disciplinary open access archive for the deposit and dissemination of scientific research documents, whether they are published or not. The documents may come from teaching and research institutions in France or abroad, or from public or private research centers.

L'archive ouverte pluridisciplinaire **HAL**, est destinée au dépôt et à la diffusion de documents scientifiques de niveau recherche, publiés ou non, émanant des établissements d'enseignement et de recherche français ou étrangers, des laboratoires publics ou privés.

COMMUNICATION

Design of lanthanide–based metal–organic frameworks with enhanced near-infrared emission

Received 00th January 20xx,
Accepted 00th January 20xx

Tu N. Nguyen,^{*a,b} Svetlana V. Eliseeva,^c Andrzej Gładysiak,^b Stéphane Petoud,^c Kyriakos C. Stylianou^{*b,d}

DOI: 10.1039/x0xx00000x

A strategy based on the use of ligand steric hindrance and metal doping is reported for the design and synthesis of near-infrared (NIR) emitting lanthanide-based metal–organic frameworks (MOFs). The lanthanide ions are free of coordinated solvents, and the resulting NIR-MOFs are highly emissive and exhibit long luminescence lifetimes.

Near-infrared (NIR) emitting materials have shown great promise for a variety of applications, ranging from optical telecommunication, biological imaging, sensing, lasers, to solar energy conversion.^{1–9} NIR luminescence is often obtained by employing lanthanide (Ln³⁺) ions; among which, Yb³⁺, Nd³⁺, and Er³⁺ are the most used lanthanides displaying NIR emission. The inherent features of Ln³⁺ ions that make them highly attractive for practical applications include their narrow bandwidth emission, high resistance to photobleaching, and the independence of the positions of the emission bands on environmental conditions.

In recent years, NIR emitting metal–organic frameworks (MOFs) have drawn much attention for their unique properties that bring together the high porosity and structural tunability of MOF platforms into lanthanide luminescence, resulting in novel multifunctional materials. Besides, MOFs are superior to molecular complexes in terms of chemical, light, and thermal stability, and mechanical properties, facilitating their use for applications.¹⁰ Up-to-date, there have already been dozens of reported MOFs based on Yb³⁺, Nd³⁺, and Er³⁺ that emit NIR luminescence, and a few with less common NIR emitting Ln³⁺ such as Pr³⁺, Ho³⁺, and Sm³⁺.¹¹ Lanthanide-based MOFs exhibit

luminescence via the ‘antenna effect’, in which the chromophoric ligands absorb a large amount of photon energy by light irradiation and transfer the corresponding energy to the accepting electronic levels of the lanthanide ion. This effect allows for addressing the limitation of low molar extinction coefficients of lanthanide ions (< 10 M⁻¹ cm⁻¹) that often results in very low luminescence intensities when the lanthanide compounds are directly excited.¹² It is worth noting that the NIR luminescence emission is significantly quenched when the lanthanide ions are located close to N–H, O–H, and C–H oscillators present on ligands and coordinated solvents due to nonradiative relaxation.¹³ One of the strategies adopted to enhance NIR luminescence quantum yield of lanthanide compounds is based on the necessity to protect the lanthanide ions from these oscillators, which is to exclude coordinated solvents, as demonstrated in lanthanide complexes.^{14–16} To further increase NIR emission, substitution of C–H bonds with lower energy and less quenching oscillators such as C–F and C–D by using perfluoro and perdeuterated ligands is a well-known approach.^{17–20}

Within the MOF field, efforts to design NIR emitting MOFs with long lifetimes and high quantum yields are rather rare. A notable attempt is the work of Chen and coworkers, which demonstrated that the enhancement of NIR emission ($\lambda_{\text{ex}} = 808$ nm) of an Er³⁺-based MOF could be achieved by replacing the ligand 1,4-benzenedicarboxylate (BDC²⁻) with its fluorinated counterpart tetrafluoroterephthalate (F₄-BDC²⁻).²¹ Yan and coworkers post-synthetically modified MIL-121 (Al(OH)(H₂btec)·H₂O, H₄btec: pyromellitic acid) by doping the MOF with Ag⁺ and Ln³⁺ ions to utilize the heavy atom effect that enhances the energy transfer process. Consequently, the NIR emission of Ag⁺/Ln³⁺@MIL-121 MOFs improved compared to the corresponding Ln³⁺@MIL-121 samples.²² Nevertheless, we believe that a more direct approach to design highly NIR emitting MOFs should at first address the issue of the solvent coordination. This represents a synthetic challenge due to the large size of Ln³⁺ ions, resulting in the high probability of binding of small solvent molecules (Fig. 1a).²³ In fact, the presence of

^a Helen Scientific Research and Technological Development Co., Ltd, Ho Chi Minh City, Vietnam.

^b Institut des Sciences et Ingénierie Chimiques (ISIC), Ecole Polytechnique Fédérale de Lausanne (EPFL Valais), 1951 Sion, Switzerland. E-mail: ngoctu.nguyen@epfl.ch

^c Centre de Biophysique Moléculaire CNRS UPR 4301, F-45071 Orléans Cedex 2, France.

^d Department of Chemistry, Oregon State University, Corvallis, Oregon 97331, USA. Email: kyriakos.stylianou@oregonstate.edu

† Electronic Supplementary Information (ESI) available: Experimental details, crystal structures, and spectroscopic data. CCDC 1946819. See DOI: 10.1039/x0xx00000x

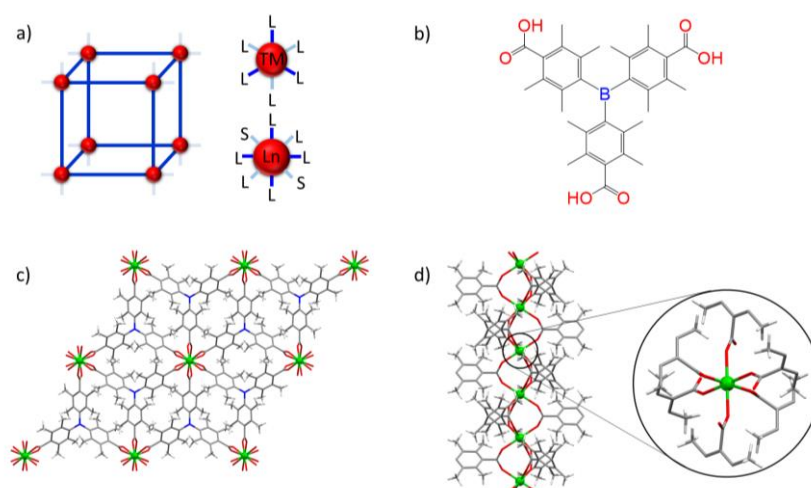


Figure 1. a) The larger size of lanthanide (Ln) ions compared to transition metal (TM) ions normally results in coordination of solvent (S) molecules in MOF structures, b) Tris(*p*-carboxylic acid)tridurylborane (H_3tctb), c) Crystal structure of **HL1-Ln** viewed along *c* axis, d) Ln channel viewed along *a* axis, and the lanthanide ion showing the absence coordinated solvent molecules. Atom colour code: green, Ln; red, O; blue, B; grey, C; white H.

coordinated solvent molecules in the first coordination sphere of Ln^{3+} is common in most reported lanthanide-based MOFs.^{24–28} Therefore, our group has been developing synthetic strategies to generate lanthanide-based MOFs with exclusion of solvent coordination.²⁹

Herein, we report the use of a sterically bulky carboxylate ligand, tris(*p*-carboxylic acid)tridurylborane (H_3tctb) (Fig. 1b), to construct a new MOF family, named **HL1-Ln**. This approach harnesses the bulkiness and hydrophobicity of the methyl CH_3 -substituents adjacent to the carboxylate groups to form a protective shell around the Ln^{3+} ions and block the coordination of solvent molecules. The syntheses, structural features, effects of metal doping, and photophysical properties of the MOFs will be presented and discussed.

HL1-Ln MOFs were synthesized using a microwave synthesizer. Nitrate salts of Ln^{3+} were mixed with H_3tctb (1:1 molar ratio) in a solvent mixture of dimethylformamide (DMF) and H_2O (2:1 v/v) at room temperature. The clear solution was then transferred to a microwave vial, sealed, and heated under microwave irradiation (power = 200 W) for 40 min at 180 °C. Crystals of **HL1-Ln** formed at the end of the reaction were collected by filtration, washed with DMF, and dried in air. This procedure allows for obtaining a series of isostructural lanthanide-MOF analogues, including those of the common NIR emitting lanthanide ions such as Yb^{3+} and Er^{3+} , as well as Eu^{3+} , Gd^{3+} , Tb^{3+} , Dy^{3+} , Ho^{3+} , Tm^{3+} , and Y^{3+} . MOFs of Ln^{3+} larger than Eu^{3+} , such as Nd^{3+} and Sm^{3+} , however, were not formed. It is worth noting that the reaction temperature of 180 °C is required to form pure **HL1-Ln** MOF products; a similar reaction with $Eu(NO_3)_3$ and H_3tctb at 120 °C gave a mixture of **HL1-Eu** and **SION105-Eu**, which was previously reported by our group.³⁰ The short reaction time of 40 min, compared to days for the solvothermal method, exemplifies the advantage of the microwave-assisted synthesis. Longer microwave radiation

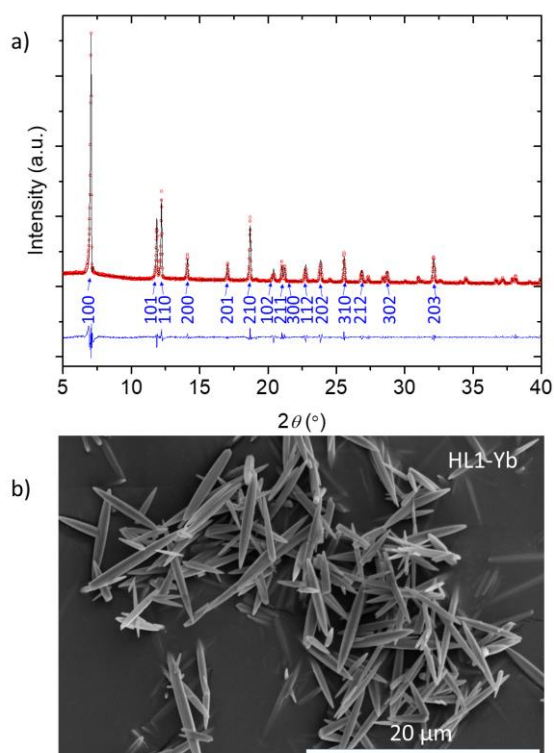


Figure 2. a) PXRD Le Bail refinement of **HL1-Eu** (space group $P\bar{3}1c$, $R_p = 6.77\%$, $R_{wp} = 9.08\%$, $a = b = 14.4934(9)$ Å, $c = 9.2724(6)$ Å, $\alpha = \beta = 90^\circ$, $\gamma = 120^\circ$; $\lambda = 1.54059$ Å). The red dots represent the experimental data, the black plots show the refined Le Bail profiles, while the blue plots represent the difference between them. Reflection positions are marked in blue, with corresponding hkl indices. b) SEM image of **HL1-Yb**.

time, e.g. 2 hours, was investigated, but the products of **HL1-Ln** remain the same.

Single-crystal X-ray diffraction data were collected on **HL1-Eu** as a representative MOF for the **HL1-Ln** family. **HL1-Eu** crystallizes in the trigonal space group $P\bar{3}1c$, with the asymmetric unit consisting of one third of the $tctb^{3-}$ ligand and one Eu atom situated on a special $2d$ position with 1/6 occupancy, and a chemical formula of $[Eu(tctb)]$. The 3-dimensional framework (Fig. 1c) is based on 1-dimensional chains of Eu^{3+} ions (Fig. 1d) linked together by the $tctb^{3-}$ ligands, within which the Eu^{3+} ions are separated by $4.6313(3) \text{ \AA}$. Every two subsequent Eu^{3+} ions are bridged within the chain by three syn-syn bridging carboxylate groups, and each Eu^{3+} ion is six-coordinate with a trigonal antiprismatic geometry which is rather unusual for Ln^{3+} ions due to the steric bulkiness of the CH_3- substituents adjacent to the carboxylate groups that prevents higher coordination numbers. As a consequence, solvent molecules do not participate to the coordination sphere of the Eu^{3+} ions (Fig. 1d). Considering the $tctb^{3-}$ ligands, 6-coordinated nodes, and the Eu^{3+} ion as 6-coordinated nodes, **HL1-Ln** has a *nia* net topology (Fig. S1, ESI†).

The needle-shape crystals of **HL1-Ln** MOFs, with sizes ranging from 10–300 μm (Fig. 2b and Fig. S2, ESI†), were collected and submitted for powder X-ray diffraction (PXRD) and Fourier-transformed infrared (FTIR) spectroscopic studies, elemental analysis, and inductively coupled plasma – optical emission spectrometry (ICP-OES) to confirm their phase purity. As shown in Fig. 2a, the experimental PXRD pattern of **HL1-Eu** can be indexed, and using the Le Bail fit, its cell parameters can be refined. The PXRD patterns of all **HL1-Ln** MOFs are in excellent agreement with the simulated ones derived from the

crystal structure of **HL1-Eu**. (Fig. S4, ESI†). In addition, the FTIR spectra of all the MOFs are nearly identical (Fig. S8, ESI†). The MOF materials are stable in aqueous solutions for at least 24 hours as confirmed by PXRD (Fig. S5, ESI†), which is expected due to the strong interaction between the hard-acidic Ln^{3+} ions and the hard-basic O atoms of the ligand. The thermogravimetric (TGA) profile of **HL1-Eu** shows that the MOF is stable up to 400 °C (Fig. S7, ESI†), which justifies the retention of its crystallinity upon heating up to ~ 400 °C during variable temperature PXRD studies (Fig. S6, ESI†).

The photophysical properties of H_3tctb and **HL1-Ln** were investigated by collecting the UV/vis absorption spectrum of H_3tctb , and excitation and emission spectra of the NIR-emitting MOFs. H_3tctb in DMF exhibits a broad absorption band attributed to $\pi \rightarrow \pi^*$ transitions located at energies corresponding to the UV region up to 380 nm, with a molar extinction coefficient of $\epsilon = 14299 \text{ M}^{-1} \text{ cm}^{-1}$ at 326 nm (Fig. S9, ESI†). To assess the organic electronic structure of the MOFs, elucidating the energies of the triplet states located on the $tctb^{3-}$ ligands, the **HL1-Gd** MOF was studied since the Gd^{3+} ion possesses a high-energy accepting electronic level (${}^6P_{7/2}$, $\sim 32000 \text{ cm}^{-1}$) that prevents energy transfer from the donating electronic levels of the $tctb^{3-}$ ligands, leading to pure ligand-centered emission. Upon excitation of the **HL1-Gd** at 360 nm, the long-lived phosphorescence originating from the triplet state located on the ligand was observed by recording emission spectra in time-resolved mode, in the solid state at 77 K and using a 50 μs delay after the excitation flash (Fig. S10, ESI†). The zero-phonon component of the phosphorescence spectrum most accurately represents the energy of the triplet state (T_1) and was determined to be $\sim 21,680 \text{ cm}^{-1}$ (461.3 nm). The T_1 level is substantially higher in energy than the emissive states of the NIR emitting lanthanides such as Yb^{3+} ($E^{Yb}({}^2F_{5/2}) = 10300 \text{ cm}^{-1}$), Er^{3+} ($E^{Er}({}^4I_{13/2}) = 6700 \text{ cm}^{-1}$), and Ho^{3+} ($E^{Ho}({}^5F_5) = 15500 \text{ cm}^{-1}$ or $E^{Ho}({}^5I_6) = 8580 \text{ cm}^{-1}$),³¹ suggesting that their luminescence in the corresponding **HL1-Ln** can be generated by energy transfer from the T_1 (Figure S13, ESI†).

Luminescence excitation and emission spectra, quantum yields (Q_{Ln}^L) and lifetimes (τ_{obs}) of the NIR emitting **HL1-Ln** ($Ln = Ho, Er, Yb$) were measured. **HL1-Ho** exhibits emission bands at 950 – 1050 nm and 1150 – 1250 nm (Fig. 3a), which can be assigned to ${}^5F_5 \rightarrow {}^5I_7$ and ${}^5I_6 \rightarrow {}^5I_8$ transitions, respectively. Unfortunately, the emission signal of **HL1-Ho** was too weak for a reliable quantitative study. Nevertheless, it is worth noting that NIR emission from Ho compounds is rarely observed.³² **HL1-Er** exhibits a typical long wavelength emission in the range of 1450 – 1600 nm, which originates from the ${}^4I_{13/2} \rightarrow {}^4I_{15/2}$ transition (Fig. 3b), whilst **HL1-Yb** displays the characteristic emission band at 980 nm due to the ${}^2F_{5/2} \rightarrow {}^2F_{7/2}$ transition (Fig. 3c). The quantum yields and luminescence lifetimes are summarized in Table 1. Notably, only a few studies of NIR emitting Ln-based MOFs report quantum yield and luminescence lifetime values. The lifetime decay curves were fitted for the bi-exponential model, which might be due to the presence of both inner and surface Ln^{3+} , and/or the exchange interactions between the lanthanide ions within the framework ($d_{Ln-Ln} \sim 4.6 \text{ \AA}$). Both **HL1-Er** and **HL1-Yb** are highly emissive

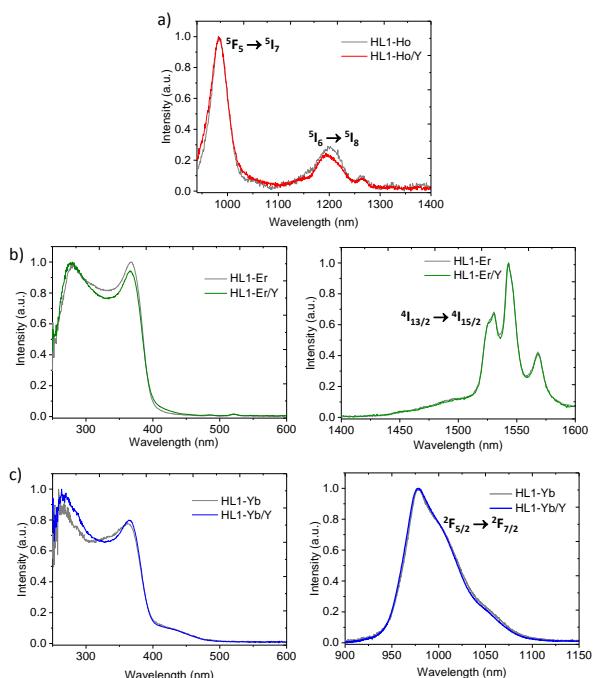


Figure 3. a) Corrected and normalized emission spectra of **HL1-Ho** and **HL1-Ho/Y**; b) and c) Corrected and normalized (left) excitation spectra upon monitoring emission at 1543 nm for **HL1-Er**, **HL1-Er/Y** or 980 nm for **HL1-Yb**, and **HL1-Yb/Y**, and (right) emission spectra of **HL1-Ln** MOFs under ligand excitation at 360 nm (solid state, room temperature).

MOFs, with the latter exhibiting higher Q_{Ln}^L and longer τ_{obs} . These values collected for **HL1-Yb** are also superior to some other Yb-based MOFs; for example, the MOF-1114-Yb compounds were reported to have $Q_{Yb}^L = 2.8 \times 10^{-2} - 4.3 \times 10^{-2}\%$, $\tau_{obs} = 0.62 - 0.67 \mu s$.²⁵ However, although τ_{obs} values for **HL1-Yb** are comparable with those reported by our group previously for **SION-100** MOF, Q_{Yb}^L is still lower for the former.²⁹ This is probably due to the relatively low sensitization efficiency of the tctb³⁻ ligands.

To investigate the effect of metal doping on the photophysical properties of **HL1-Ho**, **HL1-Er**, and **HL1-Yb**, we doped the MOFs with 50% of Y³⁺ (confirmed by the ICP-OES measurements, ESI[†]). PXRD studies showed that **HL1-Ln/Y** are isostructural to **HL1-Ln** (Fig. S4, ESI[†]). The inter- and intra chain Ln³⁺-Ln³⁺ distances in the undoped structure are around 14.5 and 4.6 Å, respectively. Doping with 50% Y³⁺ theoretically allows for an increase of the Ln³⁺-Ln³⁺ distance along the chain from ~4.6 Å to ~9.2 Å if the Ln³⁺ and Y³⁺ ions occupied alternating positions in a periodic fashion (Fig. S11). This distance is expected to significantly decrease the exchange interactions between the Ln³⁺ ions. As shown by the energy-dispersive X-ray (EDX) mapping image, the Y³⁺ ions are homogeneously distributed within the MOF bulk crystals (Fig. S3, ESI[†]). Photophysical measurements showed that **HL1-Ho/Y**, **HL1-Er/Y**, and **HL1-Yb/Y** exhibits superimposable emission spectra as those of the undoped MOFs (Fig. 3). However, when comparing the Q_{Ln}^L and τ_{obs} values of **HL1-Er/Y** and **HL1-Yb/Y** with the original values of the undoped MOFs, two opposite trends were observed (Table 1). For **HL1-Er/Y**, the τ_{obs} slightly increases, but the Q_{Er}^L is nearly six times lower than the one obtained for **HL1-Er**, indicating that the sensitization process in **HL1-Er** is very sensitive to the small change in environment around the Er³⁺ ion, whereas the concentration quenching is not as significant. For **HL1-Yb/Y**, however, both the τ_{obs} and Q_{Yb}^L are convincingly increased, suggesting the presence of concentration quenching.³³ In addition, the percentage contribution of the long lifetime reaches near unity (96%). It is worth noting that the luminescence lifetime of ~18.9 μs is among the highest values reported so far for Yb-based MOFs.^{25, 29, 34} This result clearly illustrates that by simply doping with Y³⁺, the NIR luminescence efficiencies of Yb-based MOFs can be significantly increased.

Table 1. Photophysical data for the NIR emitting MOFs under ligand excitation at room temperature^a

	τ_{obs} (μs)	Q_{Ln}^L (%)
HL1-Er	2.22(3): 93.8(5) %	3.74(7)·10 ⁻³
	0.70(3): 6.2(5) %	
HL1-Er/Y	2.80(5): 94(1)%	6.6(3)·10 ⁻⁴
	0.67(3): 6(1) %	
HL1-Yb	9.02(2): 84.0(3) %	7.2(2)·10 ⁻²
	3.31(1): 16.0(3) %	
HL1-Yb/Y	18.9(1): 96.1(5) %	1.25(1)·10 ⁻¹
	3.5(1): 3.9(5) %	

Conclusions

In conclusion, by employing ligand steric hindrance, we were able to obtain new and highly-emissive lanthanide-based MOFs that are free of solvent coordination. We demonstrated that the NIR luminescence efficiency can be further improved by doping the MOFs with Y³⁺. Future work will be the use of perdeuterated or perfluorinated ligands to prevent the quenching from the C-H groups. The strategies applied in this work can be generalized and used for other MOFs systems, and we believe that many lanthanide-based MOFs with high quantum yields and long luminescence lifetimes will soon be discovered. Our work presents a step forward towards the development of MOFs with enhanced NIR emission.

Conflicts of interest

There are no conflicts to declare.

Acknowledgements

The authors thank Dr. Pascal Schouwink and Bardiya Valizadeh for the VT PXRD and ICP-OES measurements. T.N.N thanks Helen Co., Ltd for support. K.C.S thanks the Chemistry Department at Oregon State University for support through the start-up funding. The work in France was supported by la Ligue Contre le Cancer and the Réseau "Molécules marines, métabolisme et cancer" from Cancéropôle Grand Ouest. S. P. acknowledges support from Institut National de la Santé et de la Recherche Médicale (INSERM).

Notes and references

1. A. Foucault-Collet, K. A. Gogick, K. A. White, S. Villette, A. Pallier, G. Collet, C. Kieda, T. Li, S. J. Geib, N. L. Rosi and S. Petoud, *Proc. Natl. Acad. Sci. U. S. A.*, 2013, **110**, 17199.
2. B. J. Müller, S. M. Borisov and I. Klimant, *Adv. Funct. Mater.*, 2016, **26**, 7697-7707.
3. I. Martinić, S. V. Eliseeva, T. N. Nguyen, V. L. Pecoraro and S. Petoud, *J. Am. Chem. Soc.*, 2017, **139**, 8388-8391.
4. T. N. Nguyen, F. M. Ebrahim and K. C. Stylianou, *Coord. Chem. Rev.*, 2018, **377**, 259-306.
5. G. Bai, Z. Yang, H. Lin, W. Jie and J. Hao, *Nanoscale*, 2018, **10**, 9261-9267.
6. R. Xiong, D. Mara, J. Liu, R. Van Deun and K. E. Borbas, *J. Am. Chem. Soc.*, 2018, **140**, 10975-10979.
7. S. Shuvaev and D. Parker, *Dalton Trans.*, 2019, **48**, 4471-4473.
8. S. E. Creutz, R. Fainblat, Y. Kim, M. C. De Siena and D. R. Gamelin, *J. Am. Chem. Soc.*, 2017, **139**, 11814-11824.
9. G. Bao, S. Zha, Z. Liu, Y.-H. Fung, C.-F. Chan, H. Li, P.-H. Chu, D. Jin, P. A. Tanner and K.-L. Wong, *Inorg. Chem.*, 2018, **57**, 120-128.
10. H. Zuo, Y. Li and Y. Liao, *ACS Appl. Mater. Interfaces*, 2019, **11**, 39201-39208.
11. D. Zou, J. Zhang, Y. Cui and G. Qian, *Dalton Trans.*, 2019, **48**, 6669-6675.
12. L. Armelao, S. Quici, F. Barigelletti, G. Accorsi, G. Bottaro, M. Cavazzini and E. Tondello, *Coord. Chem. Rev.*, 2010, **254**, 487-505.

13. S. Comby and J.-C. G. Bünzli, in *Handbook on the Physics and Chemistry of Rare Earths*, eds. K. A. Gschneidner, J.-C. Bünzli and V. K. Pecharsky, Elsevier, 2007, vol. 37, pp. 217-470.
14. C. Y. Chow, S. V. Eliseeva, E. R. Trivedi, T. N. Nguyen, J. W. Kampf, S. Petoud and V. L. Pecoraro, *J. Am. Chem. Soc.*, 2016, **138**, 5100-5109.
15. T. N. Nguyen, C. Y. Chow, S. V. Eliseeva, E. R. Trivedi, J. W. Kampf, I. Martinić, S. Petoud and V. L. Pecoraro, *Chem. Eur. J.*, 2018, **24**, 1031-1035.
16. K. M. Ayers, N. D. Schley and G. Ung, *Chem. Commun.*, 2019, **55**, 8446-8449.
17. C. Doffek, N. Alzakhem, M. Molon and M. Seitz, *Inorg. Chem.*, 2012, **51**, 4539-4545.
18. J.-Y. Hu, Y. Ning, Y.-S. Meng, J. Zhang, Z.-Y. Wu, S. Gao and J.-L. Zhang, *Chem. Sci.*, 2017, **8**, 2702-2709.
19. Y. Ning, J. Tang, Y.-W. Liu, J. Jing, Y. Sun and J.-L. Zhang, *Chem. Sci.*, 2018, **9**, 3742-3753.
20. W. Wu, X. Zhang, A. Y. Kornienko, G. A. Kumar, D. Yu, T. J. Emge, R. E. Riman and J. G. Brennan, *Inorg. Chem.*, 2018, **57**, 1912-1918.
21. B. Chen, Y. Yang, F. Zapata, G. Qian, Y. Luo, J. Zhang and E. B. Lobkovsky, *Inorg. Chem.*, 2006, **45**, 8882-8886.
22. J.-N. Hao and B. Yan, *J. Mater. Chem. A*, 2015, **3**, 4788-4792.
23. C. Serre, F. Pelle, N. Gardant and G. Ferey, *Chem. Mater.*, 2004, **16**, 1177-1182.
24. Z. Guo, H. Xu, S. Su, J. Cai, S. Dang, S. Xiang, G. Qian, H. Zhang, M. O'Keeffe and B. Chen, *Chem. Commun.*, 2011, **47**, 5551-5553.
25. T.-Y. Luo, C. Liu, S. V. Eliseeva, P. F. Muldoon, S. Petoud and N. L. Rosi, *J. Am. Chem. Soc.*, 2017, **139**, 9333-9340.
26. Y. Zhu, L. Wang, X. Chen, P. Wang, Y. Fan and P. Zhang, *J. Solid State Chem.*, 2017, **251**, 248-254.
27. D. F. Sava Gallis, L. E. S. Rohwer, M. A. Rodriguez, M. C. Barnhart-Dailey, K. S. Butler, T. S. Luk, J. A. Timlin and K. W. Chapman, *ACS Appl. Mater. Interfaces*, 2017, **9**, 22268-22277.
28. X. Lian, D. Zhao, Y. Cui, Y. Yang and G. Qian, *Chem. Commun.*, 2015, **51**, 17676-17679.
29. T. N. Nguyen, G. Capano, A. Gładysiak, F. M. Ebrahim, S. V. Eliseeva, A. Chidambaram, B. Valizadeh, S. Petoud, B. Smit and K. C. Stylianou, *Chem. Commun.*, 2018, **54**, 6816-6819.
30. S. Shyshkanov, T. N. Nguyen, F. M. Ebrahim, K. C. Stylianou and P. J. Dyson, *Angew. Chem. Int. Ed.*, 2019, **58**, 5371-5375.
31. W. T. Carnall, P. R. Fields and K. Rajnak, *J. Chem. Phys.*, 1968, **49**, 4424-4442.
32. J. Zhang, P. D. Badger, S. J. Geib and S. Petoud, *Angew. Chem. Int. Ed.*, 2005, **44**, 2508-2512.
33. S. Omagari, T. Nakanishi, Y. Hirai, Y. Kitagawa, T. Seki, K. Fushimi, H. Ito and Y. Hasegawa, *Eur. J. Inorg. Chem.*, 2018, **2018**, 561-567.
34. C. Liu, S. V. Eliseeva, T.-Y. Luo, P. F. Muldoon, S. Petoud and N. L. Rosi, *Chem. Sci.*, 2018, **9**, 8099-8102.